FLUID-STRUCTURE INTERACTION ANALYSIS OF LIQUID STORAGE STRUCTURES

액체 저장구조물의 유체－구조물 상호작용 해석

尹 楨 邦* 김 진 웅***
Yun, Chung－Bang Kim, Jhin－Wung
金 永 晳** 서 정 문***
Kim, Young－Surck Seo, Jeong－Mun
金 裁 民** 田 英 善***
Kim, Jae－Min Choun, Young－Sun

요 약

본 논문에서는 직사각형 형태의 사용후 핵연료 저장구조물에 대한 내진해석을 다루었다. Eulerian과 Lagrangian의 두가지 해석방법을 사용하여, 그 결과를 비교하였다. Eulerian 접근방법에서는 유체 운동에 대한 Laplace 방정식의 경계치 문제를 푼 반면, Lagrangian 접근방법에서는 저장구조물은 고체 유한요소로 모형화 하였고, 내부유체는 유체 유한요소로 모형화 하였다. 유체영역을 모형화 하는데 사용된 유체요소의 강성을 적절히 산정하기 위하여 (1×1)의 감차적분을 적용하였다. 응답스펙트럼해석법으로 유체--구조물 상관관계의 내진해석을 수행한 결과, 두 접근방법으로 구한 벽면에 작용하는 유동압이 잘 일치함을 알 수 있었다. 또한 벽면 유연성의 영향을 포함할 경우, 지진 발생시 벽면에 작용하는 유동압이 크게 증가할 수 있음을 알았다.

Abstract

In this paper, liquid sloshing effects in rectangular storage structures for spent fuel under earthquake loadings are investigated. Eulerian and Lagrangian approaches are presented. The Eulerian approach is carried out by solving the boundary value problem for the fluid motion. In the Lagrangian approach, the fluid as well as the storage structure is modelled by the finite element method. The fluid region is discretized by using fluid elements. The (1×1)-reduced integration is carried out for constructing the stiffness matrices of the fluid elements. Seismic analysis of the coupled system is carried out by the response spectra method. The numerical results show that the fluid forces on the wall obtained by two approaches are in good agreements. By including the effect of the wall flexibility, the hydrodynamic forces due to fluid motion can be increased very significantly.

* 정회원, 한국과학기술원 토목공학과 교수
** 정회원, 한국과학기술원 토목공학과 박사과정
*** 한국원자력연구소 구조부

이논문에 대한 토론을 1993년 3월 31일까지 본학회에 보내주시면 1993년 9월호에 그 결과를 게재하겠습니다.

1. INTRODUCTION

The safety of the spent fuel storage structures is extremely important, because the failure of the structures, containing cooling water and spent fuel which are of high level in radioactivity, may have disastrous consequences on lives and environments. Seismic excitation is the most important force to be considered in the design of those structures. The objectives of this study is to develop efficient methods for seismic analysis of the structures. The study focuses on the fluid-structure interactions including the effect of the wall flexibility of the structures.

There are two types of approaches for the solution of the coupled systems of the structure and fluid. One is the Eulerian approach, in which the fluid motion is formulated in terms of velocity potential : see Housner(1957), Veletsos (1974), Epstein(1976), Balendra(1982), Haroun (1983 and 1984) and Yun(1986). The other is the Lagrangian approach, in which the fluid may be treated as a solid with zero shear modulus : see Sundqvist(1983) and Chen(1990). In this study, both Eulerian and Lagrangian approaches are presented. The Eulerian approach is carried out by solving the boundary value problem for the fluid motion and applying Navier-Stokes equation for the hydrodynamic forces on the wall. In the Lagrangian approach, the storage structure and the contained fluid are modelled by the finite element method, utiliz ing a general purpose structural analysis program ADINA(1984). The fluid region is discretized by using the fluid elements. The gravity effect on the sloshing motion is represented by using a series of equivalent vertical springs along the free surface. The (1×1)-reduced integration is carried out for constructing the stiffness matrices of the fluid elements. Dynamic analysis of the coupled system is carried out for the earthquake loadings by the response spectra method.

The numerical results of several example cases indicate that the fluid forces on the wall obtained by two approaches are in good agreements. It has been also found that the effect of the flexibility of the wall is very important. By including the effect, the base shear and base moment of the structure can be increased very significantly.

2. EULERIAN APPROACH

2.1 Modelling of rectangular storage structures

The storage structures are assumed to be rigidly mounted onto the bases on the ground and partially filled with fluid as shown in Figure 1. The behaviors of the structures during earthquake are basically 3-dimensional. However, for the computational simplicity, the 2-dimensional structure as shown in Figure 2 is considered in this study. The walls of the structures are modelled by using beam elements. The equivalent bending rigidity of the wall is determined in such a way that the fundamental natural frequency of the 3-dimensional structure may be maintained. In the actual analysis, only a half of the fluid-structure system is considered, because the motion of the system under horiz

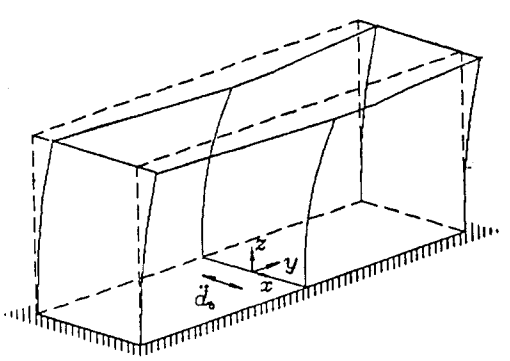

Figure 1. Rectangular storage structure.

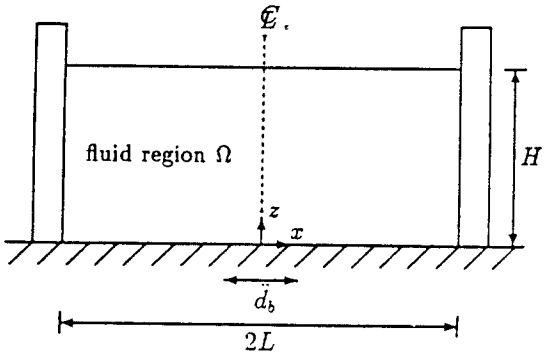

Figure 2. 2-dimensional model of a rectangular storage structure.

ontal earthquake loading is anti-symmetric with respect to the vertical plane at the center.

2.2 Velocity potential and hydrodynamic forces

For the irrotational flow of an incompressible inviscid fluid, the velocity potential, $\phi(x,z;t)$, satisfies the Laplace equation in the fluid region.

$$\nabla^2 \phi(x,z;t)=0 \text{ in } \Omega \tag{1}$$

Then, the fluid-wall boundary conditions can be expressed as follows:

$$\phi_{,x}(\pm L,z;t)=\dot{W}(z;t) \tag{2}$$
$$\phi_{,z}(x,0;t)=0 \tag{3}$$
$$\phi_{,z}(x,H;t)=\dot{\xi}(x;t) \tag{4}$$
$$\rho\dot{\phi}(x,H;t)=\rho g\xi(x;t)=0 \tag{5}$$

where $\xi(x;t)$ is the elevation of the free surface over the mean surface level; $W(z;t)$ is the horiz ontal displacement of the wall; $\phi_{,x}$ represents $\partial\phi/\partial x$; ρ is the mass density of fluid; and g is the gravitational acceleration.

The general solution for the Eq. (1), which satisfies the boundary condition on the tank wall, Eq. (2), can be expressed as,

$$\phi(x,z;t)=\sum_{n=1}^{\infty} A_n(z;t)\ \sin\ \lambda_n x+x\dot{W}(z;t) \tag{6}$$

where $\lambda_n=(2n-1)\pi/(2L)$, and $A_n(z;t)$ is the time varying coefficient of the n-th term in the sine series which is to be determined using the other boundary conditions. The free surface elevation can be also expressed in terms of the sine series as,

$$\dot{\xi}(x;t)=\sum_{n=1}^{\infty} \eta_n(t)\ \sin\ \lambda_n x \tag{7}$$

where $\eta_n(t)$ represents the generalized free surface amplitude associated with sin $\lambda_n x$.

Substituting Eqs. (6) and (7) into Eqs. (1), (3), (4) and (5), one can obtain expressions for $A_n(z;t)$ in terms of $\dot{W}(z;t)$ and $\eta_n(t)$. The horiz ontal displacement of the wall is represented by using third order polynomial of z within each beam element. Consequently, the deformation of the whole wall section is represented by much higher order terms. However, it is not practical to use the same interpolation functions to describe the fluid boundary condition along the wall, because the liquid motion is mostly associated with the low frequency vibration modes. Hence, an approximate shape which is a third order polynomial function through the depth of the contained fluid is used to obtain $A_n(z;t)$ in this study. The approximate shape, $\overline{W}(z;t)$, is determined by the least square fitting of the horiz ontal displacements of the beam at the nodes, $\{w(t)\}$, as follows,

$$W(z;t)\simeq \overline{W}(z;t)=\{P(z)\}^T\ [R]\{w(t)\} \tag{8}$$

where $\{P(z)\}^T=<1,z,z^2,z^3>$, and the coefficient matrix $[R]$ can be obtained from the z-coordinates of the nodes below free surface.

Once the solution for $A_n(z;t)$ is obtained, the velocity potential can be expressed into two parts as,

$$\phi(x,z;t)=\phi_I(x,z;\{\dot{w}(t)\})$$
$$+\phi_C(x,z;\int_0^t \{\eta(\tau)\}d\tau) \tag{9}$$

where ϕ_I and ϕ_C may be considered as the impulsive and the convective components of the velocity potential, respectively.

Substituting Eq. (9) into the free surface boundary conditions, one can obtain the relationship between $\{\eta\}$ and $\{\ddot{w}\}$ as,

$$[M_{ff}]\{\ddot{\eta}\}+[K_{ff}]\{\eta\}=[S]\{\ddot{w}\} \tag{10}$$

where diagonal matrices $[M_{ff}]$ and $[K_{ff}]$ can be interpreted as mass and stiffness matrices associated with the free surface motion; and $[S]$ is the coefficient matrix of the exciting force associated with the wall motion.

Using Eq. (9) and Navier-Stokes equation, the hydrodynamic pressure exerted on the wall can be expressed in terms of velocity potential. Then, using the virtual work principle, the nodal hydrodynamic force vector, $\{F\}$, can be obtained as,

$$\{F\}=-[M_a]\{\ddot{w}\}-[S]^T\{\eta\} \tag{11}$$

where $[M_a]$ is the hydrodynamic added mass matrix associated with the horizontal movement of the liquid; and $[S]$ is the matrix relating the horizontal force on the wall with the free surface motion. It can be easily shown that the matrices $[S]$ in Eqs. (10) and (11) are identical.

2.3 Equation of motion of fluid-structure system Combining Eqs. (10) and (11), the equation of the fluid-structure system can be obtained as,

$$\begin{bmatrix} M_{ss}+\bar{M}_a & 0 \\ -\bar{S} & M_{ff} \end{bmatrix}\begin{Bmatrix} \ddot{d} \\ \ddot{\eta} \end{Bmatrix}+\begin{bmatrix} K_{ss} & \bar{S}^T \\ 0 & K_{ff} \end{bmatrix}\begin{Bmatrix} d \\ \eta \end{Bmatrix}=\begin{Bmatrix} R_e \\ 0 \end{Bmatrix} \tag{12}$$

where $\{d\}$ is the nodal displacement vector of the wall; $\{R_e\}$ is the vector representing the reaction at the base; $[\bar{M}_a]$ and $[\bar{S}]$ are the matrices corresponding to $[M_a]$ and $[S]$ but with proper dimensions. Decomposing the displacement vector $\{d\}$ into the components at the base $\{d_b\}$ and at the free nodes $\{d_w\}$, Eq. (12) can be rewritten as,

$$\begin{bmatrix} M_{bb} & M_{bw} & 0 \\ M_{wb} & M_{ww} & 0 \\ -\bar{S}_b & -\bar{S}_w & M_{ff} \end{bmatrix}\begin{Bmatrix} \ddot{d}_b \\ \ddot{d}_w \\ \ddot{\eta} \end{Bmatrix}+\begin{bmatrix} K_{bb} & K_{bw} & \bar{S}_b^T \\ K_{wb} & K_{ww} & \bar{S}_w^T \\ 0 & 0 & K_{ff} \end{bmatrix}\begin{Bmatrix} d_b \\ d_w \\ \eta \end{Bmatrix}=\begin{Bmatrix} R_e \\ 0 \\ 0 \end{Bmatrix} \tag{13}$$

From Eq. (13), it can be observed that the coefficient matrices are unsymmetric due to the presence of the matrix $[\bar{S}]$ representing the coupling effect between the surface wave motion and the wall motion. Therefore the extraction of the gigenvalues and eigenvectors as well as the solution of the coupled equation becomes extremely difficult. Owing mainly to the difficulty, the coupling terms have been commonly omitted in many investigations: see Veletsos(1974) and Haroun(1983). In the present study, however, Eq. (13) is transformed. Substituting for $\{\ddot{d}_w\}$, determined from the second row of Eq. (13), the third row of the same equation becomes.

$$\begin{aligned}&[\bar{S}_w M_{ww}^{-1}M_{wb}-\bar{S}_b]\{\ddot{d}_b\}+[M_{ff}]\{\ddot{\eta}\}\\&+[\bar{S}_w M_{ww}^{-1}K_{wb}]\{d_b\}+[\bar{S}_w M_{ww}^{-1}K_{ww}]\{d_w\}\\&+[K_{ff}+\bar{S}_w M_{ww}^{-1}\bar{S}_w^T]\{\eta\}=\{0\}\end{aligned} \tag{14}$$

Premultiplying the second row of Eq. (13) by $[K_{ww}M_{ww}^{-1}]$ yields

$$\begin{aligned}&[K_{ww}M_{ww}^{-1}M_{wb}]\{\ddot{d}_b\}+[K_{ww}M_{ww}^{-1}M_{ww}]\{\ddot{d}_w\}\\&+[K_{ww}M_{ww}^{-1}K_{wb}]\{d_b\}+[K_{ww}M_{ww}^{-1}K_{ww}]\{d_w\}\\&+[K_{ww}M_{ww}^{-1}\bar{S}_w^T]\{\eta\}=\{0\}\end{aligned} \tag{15}$$

Combining the first row of Eq. (13) with Eqs. (14) and (15) leads to

$$\begin{bmatrix} M_{bb} & M_{bw} & 0 \\ K_{ww}M_{ww}^{-1}M_{wb} & K_{ww} & 0 \\ \bar{S}_w M_{ww}^{-1}M_{wb}-\bar{S}_b & 0 & M_{ff} \end{bmatrix}\begin{Bmatrix} \ddot{d}_b \\ \ddot{d}_w \\ \ddot{\eta} \end{Bmatrix}$$

$$+\begin{bmatrix} K_{bb} & K_{bw} & \bar{S}_b^T \\ K_{ww}M_{ww}^{-1}K_{wb} & K_{ww}M_{ww}^{-1}K_{ww} & K_{ww}M_{ww}^{-1}\bar{S}_w^T \\ \bar{S}_wM_{ww}^{-1}K_{wb} & \bar{S}_wM_{ww}^{-1}K_{ww} & K_{ff}+\bar{S}_wM_{ww}^{-1}\bar{S}_w^T \end{bmatrix}\begin{Bmatrix} d_b \\ d_w \\ \eta \end{Bmatrix} = \begin{Bmatrix} R_r \\ 0 \\ 0 \end{Bmatrix} \tag{16}$$

By expressing the displacement vector of the free nodes, $\{d_w\}$, as the sum of the ground movement, $\{d_b\}$, and the relative displacement to the ground movement, $\{d_r\}$, i.e.,

$$\{d_w\}=[I,I,\cdots,I]^T\{d_b\}+\{d_r\} \tag{17}$$

the following equation with symmetric matrices can be obtained from the second and the third rows of Eq. (16),

$$\begin{bmatrix} K_{ww} & 0 \\ 0 & M_{ff} \end{bmatrix}\begin{Bmatrix} \ddot{d}_r \\ \ddot{\eta} \end{Bmatrix}+\begin{bmatrix} K_{ww}M_{ww}^{-1}K_{ww} & K_{ww}M_{ww}^{-1}\bar{S}_w^T \\ \bar{S}_wM_{ww}^{-1}K_{ww} & K_{ff}+\bar{S}_wM_{ww}^{-1}\bar{S}_w^T \end{bmatrix}\begin{Bmatrix} d_r \\ \eta \end{Bmatrix}$$
$$=-[M_e]\{\ddot{d}_b\} \tag{18}$$

where $[M_e]$ is the effective mass matrix for the base movement as,

$$[M_e]=\begin{bmatrix} K_{ww}M_{ww}^{-1}M_{wb}+K_{ww}[I,I,\cdots,I]^T \\ \bar{S}_wM_{ww}^{-1}M_{wb}-\bar{S}_b \end{bmatrix} \tag{19}$$

From the Eq. (18), the natural frequencies and the mode shapes of the fluid-structure system can be readily computed. Then, the seismic response can be calculated by the response spectra method utilizing mode superposition.

3. LAGRANGIAN APPROACH

In this approach, the contained fluid as well as the storage structure is modelled by the finite element method. A general purpose structural analysis program ADINA is utilized for this analysis. As in the Eulerian approach described in the previous section, the fluid-structure interaction analysis is carried out by using 2-dimensional model. Plane strain conditions are assumed for the analysis against the horizontal earthquake excitations. The walls of the storage structure are modelled by using 4-noded solid elements. The fluid region is represented by utilizing 4-noded fluid elements.

The fluid elements used are equivalent to the solid elements with zero shear modulus but with an appropriate bulk modulus for the compressibility of the contained fluid. The (1×1)-reduced integration is carried out for constructing stiffness matrices of the fluid elements, since the (2×2)-normal integration of the 4-noded fluid elements causes overestimations of the stiffness of the fluid elements. The (1×1)-reduced integration gives constant pressure within an element and no stiffness against deformation shape without volume change. Consequently, spurious zero energy modes may be produced in the modal analysis. In this study, the spurious modes are identified based on the results of the modal analysis, and they are disregarded in the dynamic response analysis.

The effect of the restoring force on the free surface due to gravity, which is associated with Eq. (5), can be represented by a series of vertical equivalent springs. When a quiescent free surface is disturbed by a vertical displacement, ξ, the restoring forces, f, due to the pressure change and the stiffness of the corresponding equivalent spring, k, can be evaluated as

$$f=\rho\ g\ \xi\ dS \tag{20}$$
$$k=f/\xi=\rho\ g\ dS \tag{21}$$

where dS is an infinitesimal area of the free surface.

The relative motion of the fluid along the wall is allowed only in the tangential direction to the wall as shown in Figure 3.

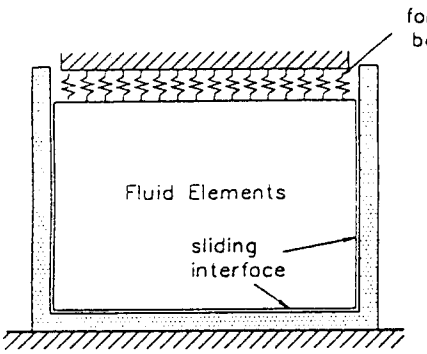

Figure 3. Finite element modelling for a flexible wall case.

4. NUMERICAL EXAMPLES AND DISCUSSIONS

4.1 Properties of example cases

Three cases of reinforced concrete structures for storage of spent fuel are investigated. The widths of the structures($2L$) are taken as 12, 30 and 60m, respectively. The wall thickness (h) is taken to be 1.2m for three structures. The fluid is assumed to be filled upto 13m above the base.

The material properties of the concrete storage structures are : Young's modulus(E)=19.6 GPa, Poisson's ratio(ν)=0.2, and mass density(ρ_s)= 2.4×10^3Kg/m^3. The properties of fluid elements are : bulk modulus(K)=2.0 GPa, and mass density (ρ)=1.0×10^3Kg/m^3.

For the seismic response analysis, the design response spectrum for the horizontal direction recommended by US NRC Regulatory Guide 1.60(1973) is used. The peak ground acceleration is taken as 0.2g, and the modal damping ratio is 0.5 percent for each mode.

4.2 Free vibration analysis

For the seismic excitations in the horizontal direction, only the anti-symmetric modes of the fluid sloshing and the structural motions contribute to the dynamic response. The frequencies of the anti-symmetric sloshing modes computed for three structures are listed in Table 1. Good agreements can be observed between the results by different approaches. It is also found that the effect of wall flexibility to the sloshing frequencies are negligible. The natural frequencies of the anti-symmetric structural modes are also evaluated. The added mass effect is included in the analysis. The first two frequencies are shown in Table 2. Fairly good agreements between the results by the Eulerian and Lagrangian approaches can be observed.

Table 2. Frequencies of anti-symmetric structural modes(Hz)

Width	Natural Frequency	Eulerian	Lagrangian
12m	w_1^{str}	3.3	2.8
	w_3^{str}	20.7	18.4
30m	w_1^{str}	3.2	3.0
	w_3^{str}	19.9	17.0
60m	w_1^{str}	3.3	3.0
	w_3^{str}	20.0	16.7

Table 1. Frequencies of anti-symmetric sloshing modes(Hz)

Width	Natural Frequency	Rigid wall			Flexible wall	
		Eulerian	Lagrangian	Housner	Eulerian	Lagrangian
12m	w_1^{slo}	0.26	0.26	0.26	0.26	0.26
	w_3^{slo}	0.44	0.36	0.44	0.44	0.36
30m	w_1^{slo}	0.15	0.15	0.15	0.15	0.15
	w_3^{slo}	0.28	0.24	0.28	0.28	0.24
60m	w_1^{slo}	0.09	0.09	0.09	0.09	0.09
	w_3^{slo}	0.19	0.20	0.19	0.19	0.20

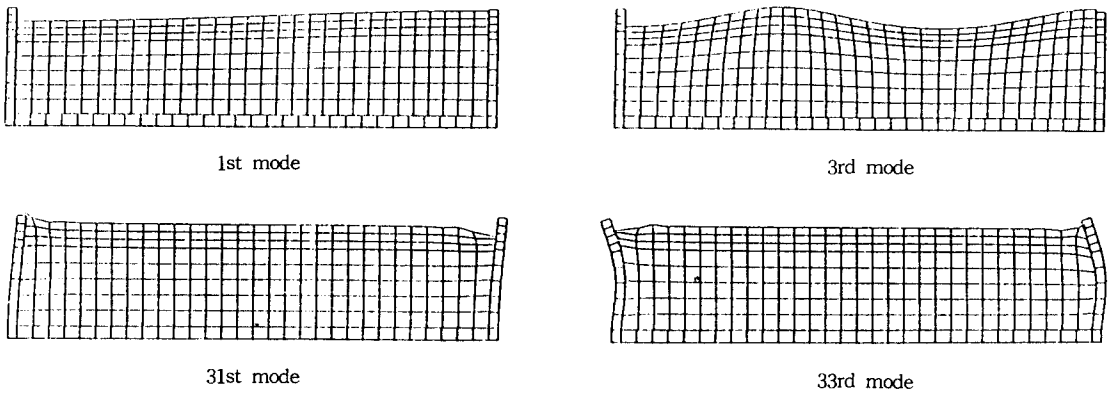

Figure 4. Anti-symmetric mode shapes for the sloshing and the structural modes of a flexible wall

From the results of the Lagrangian approach utilizing the finite element idealizations both for the structure and the fluid, the first 29 modes are found to be the sloshing modes. The first two anti-symmetric structural modes are the 31st and 33rd modes as shown in Figure 4. The corresponding natural frequencies are found to be 3.0 and 17.0 *Hz* for the structure of 30m width. These values are slightly less than those (3.2 and 19.9 *Hz*) obtained by the Eulerian approach. The discrepancies may be cuased by different ways of modelling the wall structures : i.e., beam elements in the Eulerian approach and plane strain elements in the Lagrangian approach.

4.3 Free surface elevation

Table 3 shows the maximum free surface elevation obtained by the Eulerian and the Lagrangian approaches. Maximum elevation mainly depends on the first sloshing mode. The effect of the wall flexibility on the sloshing motion is found to be negligible. The results obtained by the Lagrangian approach are in good agreements with those by the Eulerian and the Housner's methods.

Table 3. Maximum free surface elevation(m)

Width	Eulerian	Lagrangian	Housner
12m	0.91(0.91)	0.97(0.96)	−(1.27)
30m	1.14(1.13)	1.14(1.13)	−(1.29)
60m	1.13(1.13)	1.12(1.12)	−(1.04)

Note : The values in the parentheses are obtained from rigid wall cases, the others from flexible wall cases.

4.4 Base shear and base moment

The maximum shear and bending moments hydrodynamically induced at the bases of the walls are evaluated, and the results are shown in Tables 4 and 5. Comparisons with the results by the Eulerian approach indicate that the Lagrangian approach evaluates the convective components fairly accurately, while it tends to underestimate the impulsive components, particularly for the cases with rigid walls. However, for the cases with flexible walls, the discrepancies are found to be remarkably small i.e. less than 5 percent. It is noted that the maximum base shears and bending moments due to hydrodynamic pressure for the flexible wall cases are about 3 times greater than those for the rigid wall cases. It is because the fundamental natural frequencies of the wall structures are in the range, where the spectral accelerations

Table 4. Maximum base shear forces due to hydrodynamic pressure(KN)

Width	Eulerian approach			Lagrangian approach			Housner method			
	Convec.	Impul.	SRSS	Convec.	Impul.	SRSS	Convec.	Impul.	SRSS	ABS
12m	33	359	361	31	354	355	–	–	–	–
	(33)	(112)	(117)	(31)	(99)	(104)	(33)	(127)	(131)	(161)
30m	90	543	551	90	527	535	–	–	–	–
	(90)	(164)	(187)	(89)	(127)	(156)	(90)	(187)	(208)	(277)
60m	120	546	559	117	518	531	–	–	–	–
	(120)	(165)	(204)	(117)	(106)	(158)	(109)	(195)	(223)	(304)

Note : The values in the parentheses are for the rigid wall cases, the others are for the flexible wall cases.

Table 5. Maximum base moments due to hydrodynamic pressure($KN-m$)

Width	Eulerian approach			Lagrangian approach			Housner method			
	Convec.	Impul.	SRSS	Convec.	Impul.	SRSS	Convec.	Impul.	SRSS	ABS
12m	312	2522	2541	298	2497	2515	–	–	–	–
	(310)	(609)	(683)	(297)	(522)	(601)	(328)	(631)	(711)	(959)
30m	668	3425	3490	657	3324	3389	–	–	–	–
	(666)	(848)	(1078)	(655)	(663)	(932)	(694)	(925)	(1156)	(1619)
60m	810	3334	3431	783	3168	3263	–	–	–	–
	(810)	(844)	(1174)	(781)	(584)	(975)	(784)	(961)	(1241)	(1745)

Note : The values in the parentheses are for the rigid wall cases, the others are for the flexible wall cases.

of the input response spectrum are about 5 times of the maximum ground acceleration.

5. CONCLUSIONS

From the example analysis, it has been found that the Lagrangian approach utilizing the finite element modelling for the structure and the contained fluid yields very good results for the hydrodynamic forces on the wall, compared with those obtained by the more conventional Eulerian approach. Considering the versatility of the finite element modelling, the Lagrangian approach is judged to be a possible alternative way for the fluid-structure interaction analysis, particularly for the storage structures with complex geometries. It has been also found that the effects of the wall flexibility can be very important for the seismic analysis of the storage structures. By including these effects, the hydrodynamic forces on the wall may be amplified as much as three times of those corresponding to the rigid wall cases.

REFERENCES

1. ADINA Engineering AB, 1984. *ADINA User's Manual,* Sweden.
2. Balendra, T., Ang, K.K., Paramasivam, P. and Lee, S.L. 1982. Seismic deseign of flexible cylindrical liquid storage tanks. *Earthquake Engineering and Structural Dynamics* 10 : 477–496.
3. Chen, H.C. and Taylor, R.L. 1990. Vibration analysis of fluid-solid system using a finite element displacement formulation. *Int. J. for Numerical Methods in Engineering* 29 : 683–698.
4. Epstein, H.I. 1976. Seismic design of liquid storage tanks. *J. of Structural Division ASCE* 102 : 1659–1673.
5. Haroun, M.A. 1983. Vibration studies and tests of liquid storage tanks. *Earthquake Engineering and Structural Dynamics* 11 : 179–206.

6. Haroun, M.A. 1983. Stress analysis of rectangular walls under seismically induced hydrodynamic loads. *Bulletin of the Seismological Society of America* 74 : 1031 – 1041.
7. Housner, J.W. 1957. Dynamic pressure on accelerated fluid container. *Bulletin of the Seismological Society of America* 47 : 15 – 35.
8. Sundqvist, J. 1983. An application of ADINA to the solution of fluid-structure interaction problems. *Computers & Structures* 17 : 793 – 807.
9. U.S. NRC Regulatory Guide 1.60. 1973. *Design response spectrum for nuclear power plants.*
10. Veletsos, A.S. 1974. Seismic effects in flexible liquid storage tanks. *Proc. Int. Assoc. for Earthquake Engineering* 1 : 630 – 639.
11. Yun, C.B., Kim, Y.S., Kim, J.M., Kim, J.W., Seo, J.W. and Choun, Y.S. 1992. Fluid structure interaction analysis for spent fuel storage structures. *10th World Conference on Earthquake Engineering. Vol.*9 : 4975 – 4980.
12. Yun, C.B. and Lee, C.G. 1986. Liquid sloshing effect in flexible storage tanks. *Proc. 5th Congress Asian and Pacific Regional Division. Int. Assoc. for Hydraulic Research.* : 437 – 449.

(접수일자 : 1992. 9. 2)